Journal of Membrane Science 694 (2024) 122399

Contents lists available at ScienceDirect

Journal of Membrane Science

journal homepage: www.elsevier.com/locate/memsci

A comprehensive study on combined organic fouling and gypsum scaling in reverse osmosis: Decoupling surface and bulk phenomena

Shinyun Park [a], Mayca Saavedra [a], Xitong Liu [b], Tianshu Li [b], Bridget Anger [b], Tiezheng Tong [a,*]

[a] Department of Civil and Environmental Engineering, Colorado State University, Fort Collins, CO, 80523, United States
[b] Department of Civil and Environmental Engineering, George Washington University, Washington, D.C, 20052, United States

ARTICLE INFO

Keywords:
Reverse osmosis
Organic fouling
Mineral scaling
Combined fouling and scaling
Membrane scaling control

ABSTRACT

Reverse osmosis (RO), as an energy efficient desalination technology that is critical to mitigate water scarcity, encounters feedwater containing both organic foulants and inorganic scalants. However, comparing with extensive studies on individual fouling or scaling, our knowledge of the behavior and mechanisms associated with combined organic fouling and mineral scaling is still lacking. Due to the potential occurrence of mineral formation in both bulk solution and on the membrane surface, a complete, mechanistic understanding of combined fouling and scaling requires decoupling of surface and bulk phenomena. Herein, our study employed a comprehensive investigation to delve into the intricate interplay of gypsum scaling and organic fouling in RO process. Our systematic approach is accomplished through three sets of experiments that include static experiments and two types of dynamic experiments (i.e., (1) combined fouling and scaling, and (2) gypsum scaling on foulant-conditioned membranes). A variety of model foulants including humic acid, alginate, bovine serum albumin (BSA), and lysozyme were used to investigate the effects of foulant type. Our results demonstrate that the behavior of combined organic fouling and gypsum scaling aligns more with that of gypsum scaling on foulant-conditioned membranes rather than static experiments where bulk nucleation occurs, indicating the predominance of surface nucleation in RO. BSA exhibited a remarkable hindering effect on gypsum scaling, whereas other foulants displayed an additive effect. The lack of scaling mitigation by lysozyme suggests that molecular properties of protein must play a role in regulating the behavior of combined fouling and scaling. Results from multiple characterization techniques reveal the foulant-scalant interactions by delineating the morphological and chemical features of the fouling/scaling layers. Our study not only elucidates the mechanisms of combined organic fouling and gypsum scaling but also sheds light on potential strategies for membrane scaling control in RO desalination.

1. Introduction

Over the past four decades, the world has witnessed a global increase in water demand driven by a combination of climate change, population growth, socio-economic development, and change in consumption patterns [1]. It is concerning that approximately 10 % of the world's population resides in regions experiencing high or critical water stress [2]. To deal with the global challenge of water scarcity, membrane-based desalination technologies, particularly reverse osmosis (RO), have been adopted for fresh water production from saline waters such as seawater, brackish water, and industrial wastewater [3–5]. However, RO is constrained by membrane fouling, which significantly reduces the efficiency and increases overall operational and maintenance costs of desalination.

Among the different types of membrane fouling, organic fouling [6,7] and inorganic fouling (i.e., mineral scaling) [8,9] are recognized as the prevalent issues due to their ubiquitous presence in the feed water of desalination and in the autopsies of fouled membranes. Organic fouling occurs when organic matter such as humic substances, polysaccharides, and proteins adsorb on the membrane surface, while mineral scaling takes place when salt concentrations exceed the solubility of sparingly soluble minerals. Researchers have extensively investigated the impact of organic fouling and mineral scaling on RO membrane performance as well as the underlying mechanisms [10–13]. However, existing studies have been predominantly focusing on individual organic fouling or mineral scaling separately, thereby overlooking the scenario of

* Corresponding author.
E-mail address: tiezheng.tong@colostate.edu (T. Tong).

https://doi.org/10.1016/j.memsci.2023.122399
Received 24 November 2023; Received in revised form 23 December 2023; Accepted 29 December 2023
Available online 30 December 2023

combined fouling and scaling that is more relevant to real desalination process. Indeed, practical applications of RO desalination encounter feedwaters containing both organic foulants and inorganic scalants [14,15], which interact with each other and collectively determine the membrane performance.

There have been a few studies attempting to explain the behavior of combined fouling and scaling [16–19]. However, knowledge gaps still exist that prevent us from fully elucidating the effect of combined fouling and scaling on desalination performance and the corresponding mechanisms. First, researchers in the literature have observed inconsistent impacts of organic foulant on mineral scaling. For example, Wang et al. [16] reported that a layer of organic foulants altered the physicochemical properties of the membrane surface and led to more significant flux decline compared to the pristine membrane during gypsum scaling. However, a contrasting observation emerged from another study [17], where the protein-conditioned membrane exhibited a slower flux drop than the pristine membrane when being exposed to gypsum-saturated feedwater. Second, mineral scaling in membrane desalination can be attributed to nucleation on the membrane surface and/or in the bulk feedwater [9,20]. Cao et al. [18] recently demonstrated that the presence of organic foulants in the bulk solution postponed the induction time of gypsum precipitation. However, whether such a mitigating effect on bulk nucleation can be translated to better performance of dynamic RO desalination remains unknown. This is largely due to the lack of comparative studies that decouple the effects of organic foulants on surface-induced mineral scaling and scale formation in the bulk solution. As a result, systematic investigations are critically needed to further elucidate the behaviors of combined fouling and scaling as well as to disentangle bulk and surface phenomena for fully elucidating the underlying mechanisms.

In this work, we performed a comprehensive investigation on combined organic fouling and gypsum scaling in RO by conducting a set of dynamic and static experiments, which decoupled the effects of organic foulants on surface-induced nucleation and bulk nucleation of gypsum. Various organic foulants including humic acid, alginate, bovine serum albumin (BSA), and lysozyme were used as the model foulants to probe the behavior of combined organic fouling and gypsum scaling as a function of foulant type. Multiple techniques characterizing morphological and chemical features of the fouling/scaling layers were employed to thoroughly understand the interplay between organic foulants and gypsum, thereby revealing the mechanisms underlying the observed behaviors. Our findings advance the mechanistic knowledge regarding combined organic fouling and gypsum scaling, shedding light on the potential strategies for membrane scaling control in RO desalination.

2. Materials and methods

2.1. Materials

Commercial thin-film composite polyamide RO membranes (BW30LE) were obtained from Dupont FILMTEC (Wilmington, DE). Sodium chloride (NaCl), calcium chloride dihydrate ($CaCl_2{\cdot}2H_2O$), sodium sulfate (Na_2SO_4), sodium hydroxide (NaOH), and hydrochloric acid (HCl) were acquired from Fisher Chemical (Hampton, NH). Humic acid, alginate, BSA, and lysozyme were selected as model organic foulants, which represent humic substances, polysaccharides, as well as negatively- and positively-charged proteins, respectively. These model organic foulants were purchased from Sigma-Aldrich (St. Louis, MO). A water purification system (Millipore, Burlington, MA) was employed to produce deionized (DI) water (18.2 MΩ).

2.2. Combined organic fouling and gypsum scaling experiments

To investigate the behaviors of combined gypsum scaling and organic fouling, both dynamic and static experiments were performed (Fig. S1, Supplementary Materials). For the dynamic experiments, a lab-scale crossflow RO system was utilized with synthetic feedwater via two different methods: (1) adding scalants and foulants into the feed reservoir simultaneously (referred to as Method 1), and (2) conditioning the membrane surface with each model organic foulant followed by gypsum scaling (referred to as Method 2, which was designed to isolate the effects of organic foulants on surface-induced nucleation of gypsum). For Method 1, the BW30LE membranes were first compacted using DI water overnight, and then the feedwater was switched to different scaling/fouling solutions as listed in Table 1. In this method, feedwater containing only organic foulants (with the addition of NaCl and $CaCl_2$ to maintain the ionic strength (IS) the same to that of gypsum-supersaturated solution) was also used to reveal the effect of individual organic fouling. For Method 2, the membranes were conditioned with solutions containing 100 mg L^{-1} of individual foulant for 20 h after the compaction step [16,21], and the feedwater containing supersaturated gypsum was induced subsequently. During the conditioning period, 141 mM of NaCl was added with the organic foulant to maintain the IS. For both methods, the feedwater containing supersaturated gypsum consisted of 24 mM $CaCl_2{\cdot}2H_2O$ and 24 mM Na_2SO_4, resulting in a saturation index (SI, defined as the natural logarithm of the ratio between ion activity product and solubility equilibrium constant, $ln\frac{IAP}{K_{sp}}$) of 0.39 for gypsum as calculated by the PHREEQC software. The details of the feedwater compositions used in this study are described in Table 1. For all the dynamic RO experiments, the system was operated with an initial permeate water flux of 30 ± 3 L m^{-2} h^{-1} and a crossflow velocity of 21.3 m s^{-1} at 22 ± 1 °C. The operating pressure varied to achieve an identical initial water flux, due to differences in water permeability among the tested membranes. Consequently, pressures of 220 ± 20 psi were applied for Method 1, while 230 ± 20 psi (for BSA- and lysozyme-conditioned membranes) and 370 ± 20 psi (for humic acid- and alginate-conditioned membranes) were used for Method 2. After the experiments, the membrane coupons were collected from the membrane cells, gently washed with DI water, and dried in air for future analyses.

Static experiments were carried out to investigate the behaviors of bulk crystallization when organic foulants were present together with supersaturated gypsum in the solution. For the control group (i.e., no organic foulants), $CaCl_2{\cdot}2H_2O$ and Na_2SO_4 solutions were prepared separately, and then mixed using a magnetic stirrer. The final mixture solution contained 42 mM $CaCl_2{\cdot}2H_2O$ and 42 mM Na_2SO_4 with the SI of gypsum at 1.08. A higher concentration of scalants (than what was used in the dynamic experiments) was selected to investigate the effect of foulants on bulk gypsum nucleation within a reasonable timeframe. In the experimental groups, organic foulants were added to the gypsum-supersaturated solutions, making the final concentration of the foulant at 20 mg L^{-1}. It is worth noting that the concentration of foulants was not increased compared to the dynamic experiments, unlike those of scalants, because a very high concentration of foulants would significantly delay the induction time [18,19], potentially prolonging the experimental duration to exceed practical lengths of the experiments. After pH adjustment to 6.5 using 1 M NaOH or 1 M HCl, the conductivity of the solution was monitored and recorded by a conductivity meter (CON2700, Oakton, Vernon Hills, IL). The conductivity value decreased as a function of time after a certain induction time (defined as the first detectable decrease in solution conductivity) because the formation of gypsum consumed the precursor ions (i.e., Ca^{2+} and SO_4^{2-}). Once the reaction reached equilibrium (as evidenced by a stable conductivity value), the precipitates were collected using a vacuum filtration system equipped with 2.5 μm filter papers (Grade 5, Whatman, Maidstone, UK). The precipitates were then dried in an oven at 50 °C for 24 h and stored under ambient condition for further characterization.

2.3. Characterization of membranes and gypsum scales

After combined organic fouling and gypsum scaling experiments, the

Table 1
Detailed compositions of feedwaters for combined organic fouling and gypsum scaling during dynamic and static experiments.

Condition	NaCl [mM]	Organic foulants [mg L^{-1}]	Na_2SO_4 [mM]	$CaCl_2{\cdot}2H_2O$ [mM]	pH	IS [mM]
Dynamic experiments						
Gypsum scaling only			24	24	6.5	144
Organic fouling only[a]	72	20		24	6.5	144
Gypsum scaling + organic fouling[a]		20	24	24	6.5	144
Foulant conditioning[b]	141	100		1	6.5	144
Static experiment						
Gypsum only			42	42	6.5	252
Gypsum + foulant		20	42	42	6.5	252

[a] Method 1.
[b] Method 2.

membrane surfaces were characterized by several techniques. The membrane surface morphologies were analyzed by scanning electron microscopy (SEM, JEOL JSM-6200F) with a 15 nm-coating of gold layer on the membrane surface. The spectra of attenuated total reflection-Fourier transform infrared (ATR-FTIR) spectroscopy were obtained using a wavelength range from 4000 cm^{-1} to 500 cm^{-1} with 32 scans of each sample by a Nicolet iS-50 spectrometer (Thermo Fisher Scientific, Waltham, MA) to analyze the surface functionality. The crystalline structures of the crystals formed on the membrane surface were characterized by X-ray diffraction (XRD, Bruker D8 Discover DaVinci, Billerica, MA. The XRD patterns were obtained within the angular range of 5° to 60° with X-ray generation at the voltage of 40 kV and the current of 40 mA. In addition, X-ray photoelectron spectroscopy (XPS, PE-5800, Physical Electronics, Chanhassen, MN) with a monochromated Al-Kα X-ray source was employed to investigate the local chemical environment of calcium. The survey spectra were collected first followed by the high-resolution spectra for carbon and calcium elements. The collected data were analyzed with the CasaXPS software (Version 2.3.25, Casa Software Ltd). All the XPS spectra were referenced to the C–C peak in C 1s spectra after calibration by assigning the value of 284.8 eV [22].

3. Results and discussions

3.1. Behaviors of combined organic fouling and gypsum scaling when foulants coexist with scalants in the feedwater

In this section, we performed RO experiments with the membranes exposed to feedwaters that contain both organic foulants and mineral scalants simultaneously, resembling the scenarios during practical desalination process. As shown in Fig. 1, the behaviors of combined organic fouling and gypsum scaling vary depending on the foulant type. When gypsum scaling occurred in the absence of any organic foulants, the water flux of RO decreased as a function of time, leading to a flux decline of ~50 % after 500-min experiments. The salt rejection rate of the RO membrane was not compromised. Rather, it increased with time (Fig. S2, Supplementary Materials), probably due to the relatively

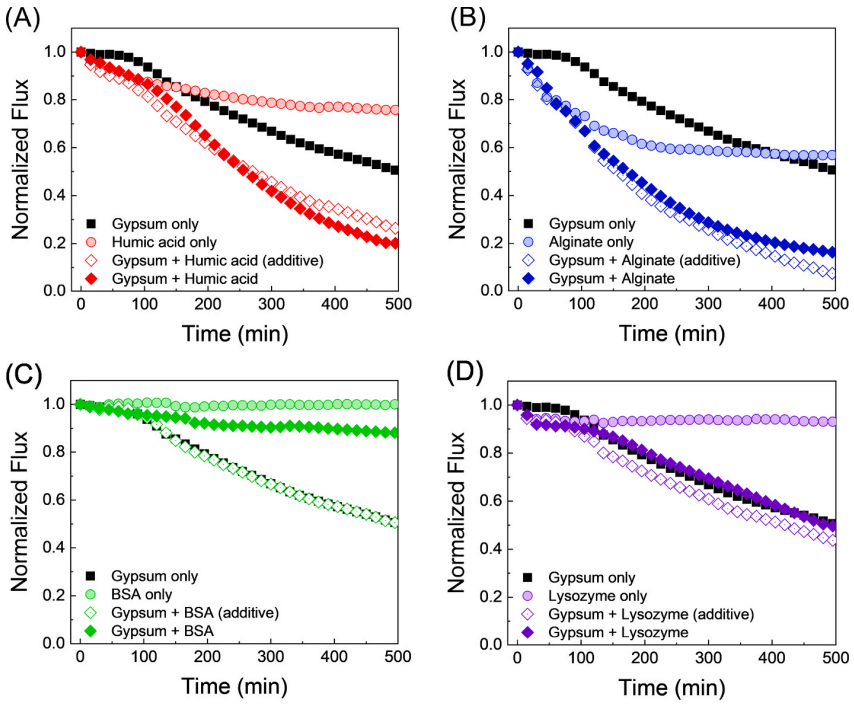

Fig. 1. Normalized water flux during combined gypsum scaling and organic fouling in RO for 500 min using the feedwater with a saturation index for gypsum at 0.39 under pH 6.5 (24 mM $CaCl_2{\cdot}2H_2O$, 24 mM Na_2SO_4, and 20 mg L^{-1} organic foulant): (A) humic acid, (B) alginate, (C) bovine serum albumin (BSA), (D) lysozyme. The label of 'Gypsum + Foulant (additive)' is referred to an additive flux curve (i.e., the mathematical summation of water flux decline rates caused by individual gypsum scaling and individual organic fouling). The RO system was operated using commercial membranes (BW30LE) at 22 ± 1 °C with an initial flux of 30 ± 3 L m^{-2} h^{-1} and a crossflow velocity of 21.3 m s^{-1}.

impermeable scale layer and the perm-selectivity trade-off (i.e., a decrease of membrane water permeability corresponds to an increase of salt rejection). When humic acid coexisted with supersaturated gypsum in the feed solution (Fig. 1A), the resultant flux decline was much faster than that caused by individual gypsum scaling. However, we noticed that individual organic fouling by humic acid in the presence of calcium ions also led to a decrease of water flux due to the complexation between calcium ions and foulants [23]. Therefore, an additive flux curve (i.e., the mathematical summation of water flux decline rates caused by individual gypsum scaling and individual organic fouling) was constructed. The water flux curve of combined humic acid fouling and gypsum scaling was nearly identical to the corresponding additive flux curve, indicating that an additive effect, rather than a synergistic effect, took place between humic acid fouling and gypsum scaling. A similarly additive interplay was observed between alginate fouling and gypsum scaling (Fig. 1B).

In contrast, the presence of BSA significantly reduced the water flux decline caused by gypsum scaling (Fig. 1C), resulting in a water flux decline of only ~10 % after 500-min experiments. The water flux of combined BSA fouling and gypsum scaling was much more stable than the corresponding additive curve. Therefore, an antagonistic effect of BSA fouling on gypsum scaling was observed. However, such an antagonistic effect was not universally applied to the interaction between gypsum scaling and protein fouling. When supersaturated gypsum coexisted with lysozyme, another protein carrying the opposite charge compared to BSA (positive charge of lysozyme vs. negative charge of BSA), the water flux curve of combined lysozyme fouling and gypsum scaling was almost identical to the additive flux curve. Therefore, the effect of organic fouling on gypsum scaling is a function of not only foulant type (e.g., humic acid, polysaccharides, and proteins) but also the molecular property (e.g., proteins of different properties) of the foulant.

To elucidate the mechanisms underlying the behaviors of combined organic fouling and gypsum scaling, we employed various techniques to characterize the scaled/fouled membranes after the scaling/fouling experiments. First, SEM was used to observe the morphologies of the gypsum scales on the membrane surface. As shown in Fig. 2A, rosette crystal morphology of gypsum, which is characteristic for gypsum scales formed in RO [22,24], was observed on the membrane after individual gypsum scaling. However, larger and more dispersed gypsum scales were found on the membranes when humic acid or alginate was present with gypsum (Fig. 2B and C). Thus, although imposing an additive effect on gypsum scaling, the presence of humic acid or alginate distorted the morphology of gypsum scale formed during RO desalination. The most notable difference was observed on the membrane surface after combined BSA fouling and gypsum scaling, where no crystals with defined shape were observed (Fig. 2D) and the membrane surface was similar to that of a pristine polyamide membrane under low magnification of SEM (Fig. 2F). This result suggests that BSA significantly hindered the formation of gypsum crystals on the membrane surface, explaining the

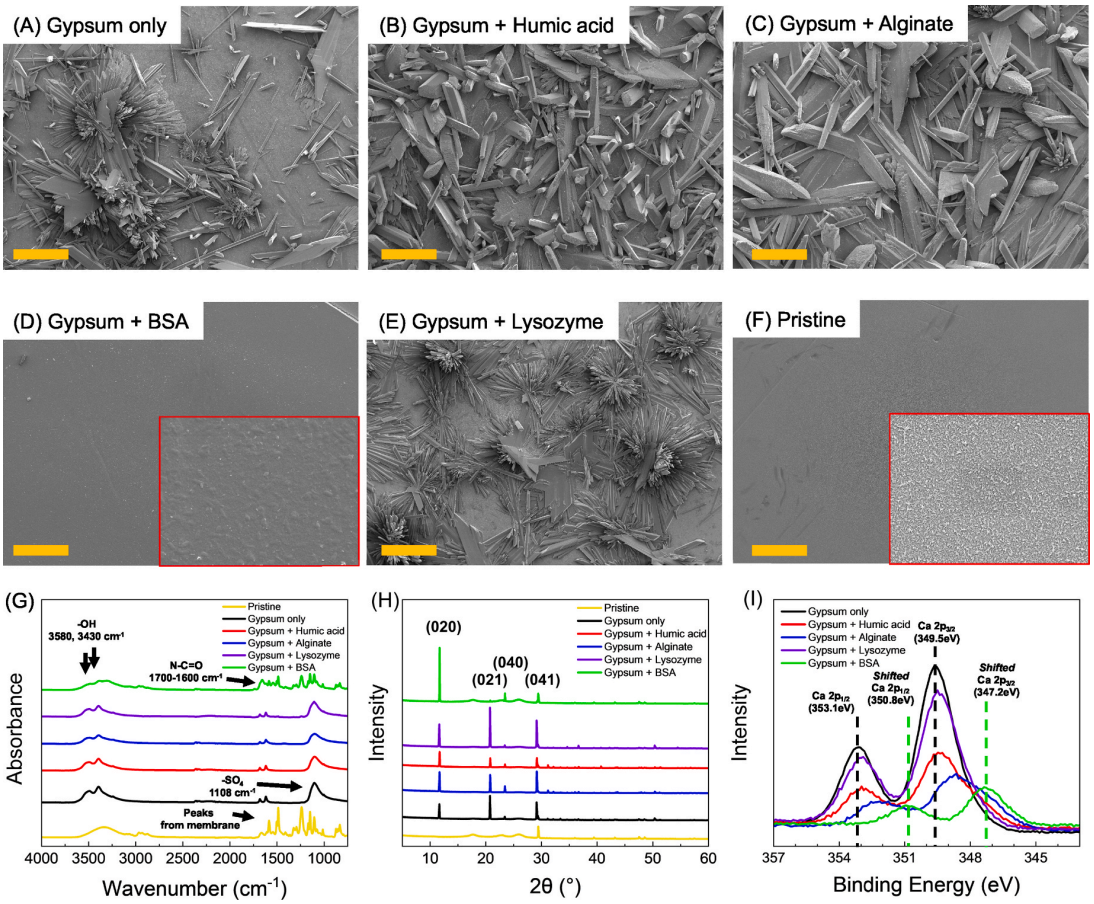

Fig. 2. Characterizations of the membranes after combined organic fouling and gypsum scaling when foulants and scalants coexist in the feedwater. (A–F) SEM images (obtained at the magnification of × 200) of the membrane surfaces from (A) gypsum only, combined gypsum scaling with (B) humic acid, (C) alginate, (D) BSA, and (E) lysozyme fouling. The image of a pristine polyamide membrane is shown in (F). The scale bars represent 200 μm and the inserted images in (D) and (F) were taken at a higher magnification (× 3000). (G–I) The spectra of the membrane surfaces obtained using (G) ATR-FTIR, (H) XRD, and (I) XPS.

antagonistic effect of BSA on gypsum scaling (Fig. 1C). In contrast, gypsum scales with rosette morphology appeared on the membrane surface after combined lysozyme fouling and gypsum scaling (Fig. 2E), which was consistent with the negligible effect of lysozyme on the water flux decline caused by gypsum scaling (Fig. 1D).

We further analyzed the membrane surfaces with ATR-FTIR spectroscopy. Characteristic peaks corresponding to –OH (3580 cm^{-1} and 3430 cm^{-1}) and $–SO_4$ (1108 cm^{-1}) functional groups of gypsum [25] were observed for the membrane after individual gypsum scaling, indicating the presence of a gypsum layer (thicker than the penetration depth of infrared irradiation) on the membrane surface (Fig. 2G). When alginate, humic acid, and lysozyme were added to the feed solutions with supersaturated gypsum, the characteristic peaks of gypsum were also clearly seen, suggesting that those organic foulants did not significantly prohibit the formation of gypsum on the membrane surface. Such results were consistent with the SEM results (Fig. 2) and the RO results where these three organic foulants were essentially posing an additive effect on gypsum scaling (Fig. 1; it is worth mentioning that lysozyme indeed exhibited a negligible effect on gypsum scaling. Thus, the term "additive effect" for lysozyme is only from the mathematical perspective). When BSA coexisted with gypsum, however, the FTIR signals for the characteristic peaks of gypsum were greatly reduced, meanwhile the characteristic peaks for polyamide membrane appeared (Fig. 2G). In addition, the peaks corresponding to N–C═O and C–N–H groups of BSA at 1700-1600 cm^{-1} and 1540 cm^{-1} [26] were intensified (Fig. S3, Supplementary Materials). Therefore, the presence of BSA led to a thinner scale layer with a lower mass density. Such a result was in accordance with the fact that gypsum particles were not observed on the membrane surface after combined BSA fouling and gypsum scaling (Fig. 2D), and that the coexistence of BSA significantly mitigated the water flux decline caused by gypsum scaling (Fig. 1C).

We also employed XRD to analyze the crystallinity of the gypsum scales formed under different conditions. As shown in Fig. 2H, characteristic peaks corresponding to various facets of gypsum crystal were observed after individual gypsum scaling. The presence of lysozyme did not change the XRD spectra, consistent with its negligible effect on gypsum scaling as shown above. Although all the characteristic peaks were clearly seen when gypsum coexisted with alginate and humic acid, these organic foulants led to differences in the crystalline structure of the formed gypsum crystals, as reflected by the alternation of relative peak intensity. For example, the peak intensity ratio of (020) to (021) facets was only 0.7 for gypsum formed in the absence of foulants, while such a ratio increased to 1.1 and 1.6 in the presence of alginate and humic acid, respectively (Table S1, Supplementary Materials). These results corroborate with the distorted morphologies of gypsum observed in Fig. 2B and C. Further, BSA posed the most significant effect on the relative intensity of XRD peaks. The peak intensity of (021) facet almost disappeared (Fig. 2H), leading to a dramatically increased peak intensity ratio of (020) to (021) facets. This indicates that BSA significantly disrupted the growth of gypsum crystals in (021) facet, while forcing gypsum to grow alternatively in the (020) facet. Given that crystals with high facet ratios exhibit flat morphologies rather than three-dimensional shapes [27], it is inferred that the presence of BSA obstructed gypsum growth in the vertical orientation, explaining the lack of defined shape of gypsum scale in Fig. 2D. Similar results were obtained when the peak intensity ratios of (040) to (041) facets were calculated (Table S1).

In addition, XPS analysis was performed to investigate the chemical environment of Ca element regarding the scaled membranes in the absence or presence of organic foulants. As shown in Fig. 2I, the high-resolution Ca 2p spectra of the membranes after gypsum scaling without any foulants exhibited the characteristic peaks of Ca $2p_{3/2}$ and Ca $2p_{1/2}$ at 353.1 eV and 349.5 eV, respectively. However, when gypsum scaling took place with organic foulants, these peaks were shifted towards lower binding energies (Table S2, Supplementary Materials). As calcium can interact with not only sulfate (SO_4^{2-}) but also carboxyl groups ($–COO^-$), these shifts are likely attributed to the formation of calcium complex with the foulants. It is known that binding energy of an element depends on the electronegativity of the nearest neighbor element [28]. The peaks were shifted to lower binding energies when calcium bound with carboxyl groups (of the organic foulants), which are less electronegative than sulfate groups. Specifically, as listed in Table S2, combined gypsum scaling with lysozyme and humic acid fouling resulted in slight shifts in peak positions compared to individual gypsum scaling. This indicates that the chemical environment of calcium element was marginally altered because of calcium interacted with COO^- of lysozyme and humic acid. Moreover, the peaks were shifted more in the presence of alginate, suggesting an increased extent of $Ca–COO^-$ binding that relates to the contribution of calcium to the formation of the foulant layer [29,30]. Furthermore, significant shifts of Ca $2p_{3/2}$ and Ca $2p_{1/2}$ binding energies to 350.8 eV and 347.2 eV were observed with the existence of BSA, indicating a substantially diminished calcium binding with sulfate (i.e., less formation of gypsum).

We further examined the XPS data by decomposing the Ca $2p_{3/2}$ peaks into subpeaks (Fig. 3) that represent different types of chemical binding regarding calcium [31–33]. In the XPS spectra of the gypsum-scaled membrane without foulants (Fig. 3A), subpeaks corresponding to both $Ca–SO_4$ and $Ca–COO^-$ bindings were observed, with much smaller areas of the $Ca–COO^-$ peaks resulted from the interaction of calcium with carboxyl groups in the polyamide layer of RO membrane. As shown in Fig. 3B-E, the areas of the subpeaks attributed to $Ca–SO_4$ and $Ca–COO^-$ bindings varied depending on the type of coexisting foulant. To indicate the contributions of these two types of bindings to Ca present in the scale layer, we calculated the relative abundance of each binding type by quantifying the areas of the corresponding peaks (Fig. 3F). The presence of BSA led to the largest abundance of $Ca–COO^-$ binding, followed by alginate, humic acid and lysozyme. This order is consistent with the order of peak shifting observed in Fig. 2I and Table S2. The same results were also obtained when the decomposition of Ca $2p_{1/2}$ peaks was performed (Figure S43A, Supplementary Materials).

We noticed that the relative abundance of calcium binding with COO^- was observed as 100 % in the case of BSA (Fig. 3F), despite the detection of gypsum by ATR-FTIR (Fig. 2G) and XRD (Fig. 2H) analyses. This discrepancy is attributed to the difference in measurement depth of different characterization methods, with XPS being a more surface-sensitive technique compared to ATR-FTIR and XRD. It has been reported that the analysis depth of XPS is typically about 5–10 nm, whereas ATR-FTIR and XRD can analyze up to a few microns in depth [34,35]. This indicates that the formation of gypsum scales in the presence of BSA did not occur on the top surface of the membrane (otherwise $Ca–SO_4$ binding from gypsum should have been observed by XPS in Fig. 3F). During combined BSA fouling and gypsum scaling, gypsum precursors and BSA were added together in the feedwater. Thus, gypsum formation and the deposition of BSA foulants on the membrane surface took place concurrently. Initially, the quantity of BSA on the membrane surface was insufficient to hinder gypsum formation. As further BSA deposition occurred, the BSA foulant layer eventually inhibited gypsum scaling (such an effect was similar to what was observed for the membrane conditioned with a BSA foulant layer, as discussed in the following section). As a result, the characteristics of gypsum were detected beneath the foulant layer while $Ca–SO_4$ binding pertaining to gypsum was not observed on the surface. This suggests that although BSA significantly disrupted gypsum crystallization, it did not completely prevent the formation of gypsum crystals within the BSA foulant layer.

3.2. The effects of foulant conditioning on the behaviors of gypsum scaling

A conditioning step was conducted for 20 h with a high concentration (100 mg L^{-1}) of model organic foulants to induce the formation of a foulant layer on the membrane surface. By doing so, the effects of organic foulants on the subsequent gypsum scaling were due to the

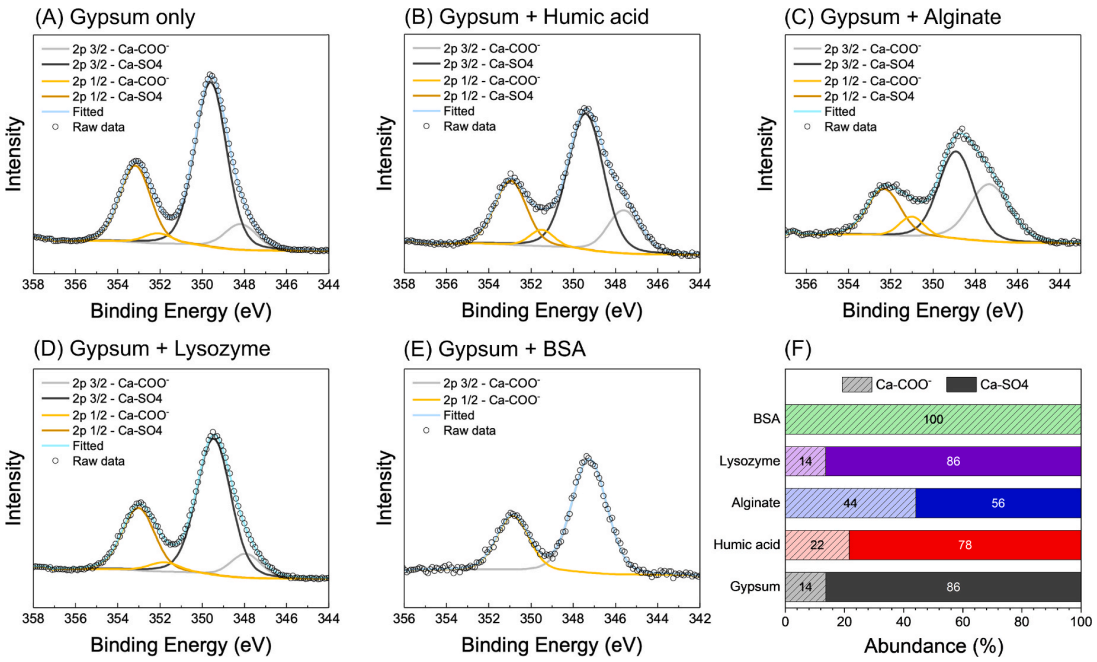

Fig. 3. High-resolution XPS spectral decompositions of Ca 2p to subpeaks corresponding to Ca–SO_4 and Ca–COO^- bindings for membranes after (A) gypsum scaling, as well as combined gypsum scaling and organic fouling using (B) humic acid, (C) alginate, (D) lysozyme, and (E) BSA. (F) Relative abundance of Ca–COO^- and Ca–SO_4 bindings by calculating the peak areas. The sum of the binding abundance is designated as 100 %.

foulant-gypsum interactions on the membrane surface (predominantly the effects of organic foulants on surface nucleation of gypsum, considering the lower free energy barrier of surface nucleation than that of bulk nucleation [9]). As shown in Fig. S5A (Supplementary Materials), the water flux in the presence of humic acid and alginate declined significantly as a function of time, while a slight flux decrease was seen for protein (i.e., lysozyme and BSA) fouling. Such flux decline behaviors of organic fouling were consistent with those reported in the literature [16,36]. ATR-FTIR analyses (Fig. S5B, Supplementary Materials) were performed on the fouled membranes to confirm the formation of foulant layers. The spectra of membranes conditioned with humic acid and alginate differed greatly from that of pristine TFC-PA membrane. For example, the peaks at 1600-1500 cm^{-1} (aromatic stretching vibration of C═C) and 1400 cm^{-1} (aliphatic CH_2 and CH_3 bending) [37] appeared for the humic acid-conditioned membrane, while the characteristic peaks at 1635 cm^{-1} and 1419 cm^{-1} (asymmetric and symmetric stretching vibrations of carboxyl groups, respectively) [38] were observed for the alginate-conditioned membrane. This indicates that thick foulant layers were formed on the membrane surface. On the other hand, the intensities of protein characteristic peaks at 1700-1600 cm^{-1} (amide I, N–C═O vibration) and 1540 cm^{-1} (amide II, C–N–H vibration) [26] were enhanced for the protein-conditioned membranes (Fig. S5B, Supplementary Materials), implying that foulant layers were also created by BSA and lysozyme.

After conditioning with organic foulants, the feedwater was switched to gypsum-saturated solutions to induce gypsum scaling. As shown in Fig. 4, conditioning with humic acid and alginate resulted in faster decrease of water flux at the early stage (e.g., the first 150 min) than the control group where gypsum scaling occurred on the pristine BW30LE membrane. However, the final water fluxes of the conditioned membranes after 500 min were higher than that of the control group. Such behaviors were attributed to the organic foulant layers, which facilitated gypsum scaling at the early stage due to cake enhanced concentration polarization (which increases the concentrations of precursor ions near the membrane surface) [39] but obstructed the crystal growth at the later stage [40]. On the other hand, lysozyme conditioning showed a

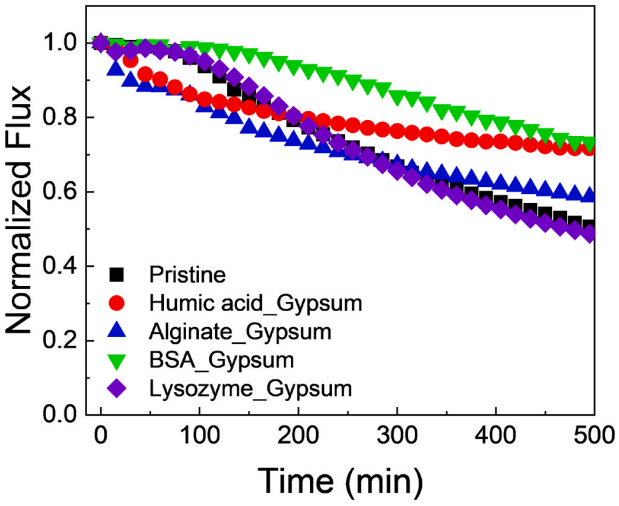

Fig. 4. Normalized water flux during gypsum scaling on the RO membranes conditioned with organic foulants (100 mg L^{-1} of foulants with 1 mM of calcium). The feedwater for gypsum scaling has a saturation index for gypsum at 0.39 under pH 6.5 (23 mM $CaCl_2{\cdot}2H_2O$, 24 mM Na_2SO_4) The RO system was operated using commercial RO membranes (BW30LE) at 22 ± 1 °C with an initial flux of 30 ± 3 L m^{-2} h^{-1} and a crossflow velocity of 21.3 m s^{-1}.

negligible effect on gypsum scaling, whereas BSA-conditioned membrane exhibited reduced gypsum scaling. Therefore, consistent with the excellent mitigating effect of BSA on gypsum scaling in combined fouling and scaling (as shown in Section 3.1), a fouling layer of BSA was also able to hinder gypsum scaling in RO.

To unravel the underlying mechanisms underlying the effects of foulant layers on gypsum scaling behaviors, several characterization techniques were employed. First, SEM images (Fig. 5A-F) were acquired

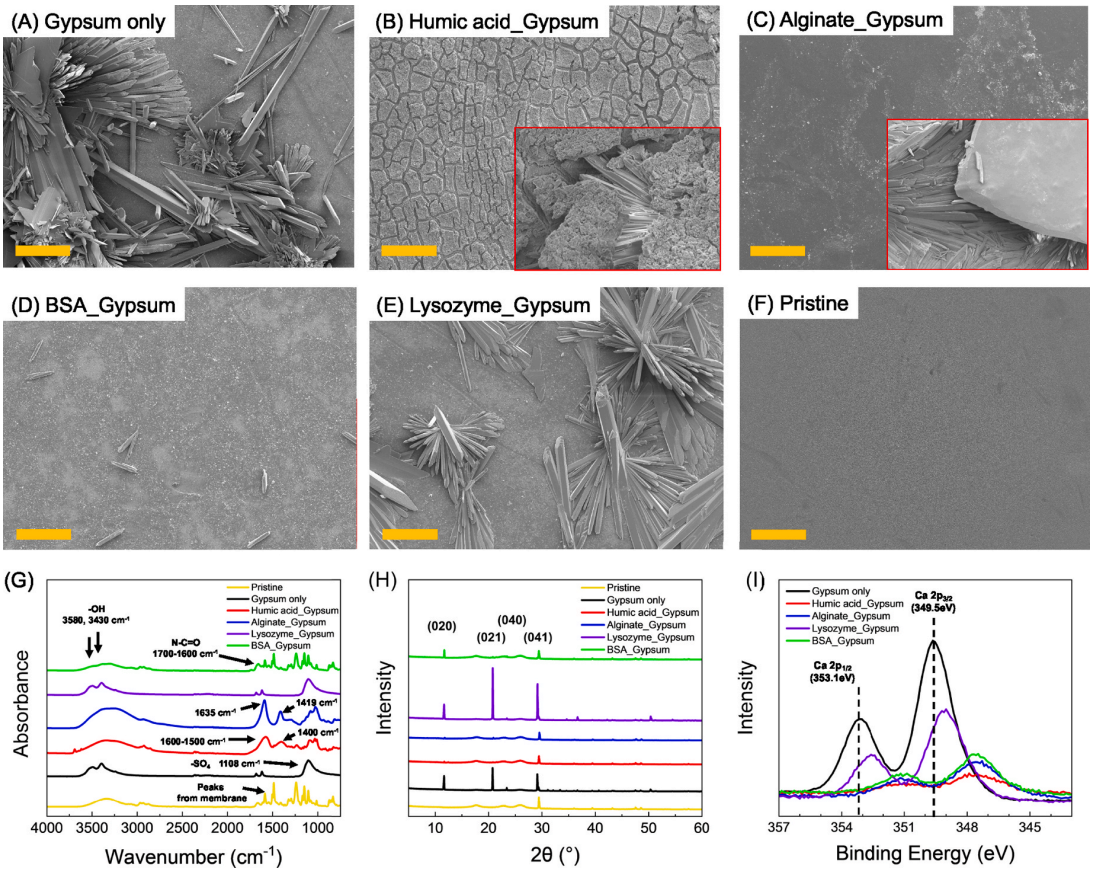

Fig. 5. SEM images (obtained at the magnification of × 200) of the membrane surfaces after gypsum scaling on (A) pristine membrane, and conditioned membranes with (B) humic acid, (C) alginate, (D) BSA, and (E) lysozyme. The pristine polyamide membrane is shown in (F). The yellow scale bar represents 100 μm and the inserted images in (B and C) were taken at a higher magnification (× 1000). Note that the inset image in C was captured after peeling off the foulant layer. Spectra of the membranes obtained using (G) FTIR, (H) XRD, and (I) XPS. (For interpretation of the references to colour in this figure legend, the reader is referred to the Web version of this article.)

from the fouled membranes after 500 min of gypsum scaling to observe the morphology of the gypsum scale. Interestingly, in contrast with the crystalline gypsum scales with clearly defined shape on pristine membrane, no massive gypsum crystals were observed on humic acid- (Fig. 5B) and alginate- (Fig. 5C) conditioned membranes, even though flux decline were witnessed during gypsum scaling. We noticed that gypsum crystals indeed formed underneath the foulant layers, as clearly shown in the inset images of Fig. 5B and C. These findings suggest that gypsum scale formation occurred at the interface between the foulant layer and the membrane surface, where the highest concentrations of scaling precursor ions was present due to cake enhanced concentration polarization (the foulant layer hindered the back-diffusion of Ca^{2+} and SO_4^{2-}). Additionally, the lack of gypsum crystals on the foulant layer surface indicates that gypsum formation was inhibited on the humic acid and alginate layer, explaining the slow flux decrease in the late stage, as displayed in Fig. 4.

For protein-conditioned membranes, gypsum scales with undefined shape and much smaller mass (than the control) were found on the BSA-conditioned membrane while rosette-like crystals were observed on lysozyme-conditioned membrane (Fig. 5D and E), generally consistent with what were observed for combined gypsum scaling and protein fouling (Fig. 2D and E). However, in the case of BSA conditioning, a few rod-shape crystals were found on the BSA foulant layer whereas crystals of defined shape were not observed on the membrane surface after combined fouling and scaling (i.e., Method 1, Fig. 2D). This difference suggests that BSA in the bulk solution influenced the surface phenomenon during combined fouling and scaling. Particularly, BSA was able to form a foulant layer on the membrane surface at the early stage of combined fouling and scaling. Once the membrane surface was covered, gypsum scaling was inhibited by the BSA layer, similar to what was observed in Method 2 of this section. However, the BSA that was still present in the feed solution contributed to the continuing formation of BSA foulant layer. As a result, gypsum scaling was fully inhibited on the membrane surface but only occurred underneath the BSA layer as described in Section 3.1. Furthermore, lysozyme in the bulk solution did not have any effect on the surface scaling behavior considering no morphological change of the gypsum crystals, which demonstrate again that foulants of the same type (i.e., protein) but different molecular properties pose varied effects on gypsum scaling.

To characterize the membranes after gypsum scaling on the conditioned membranes, ATR-FTIR analysis (Fig. 5G) was conducted. In the FTIR spectra of the humic acid- and alginate-conditioned membranes after gypsum scaling, the characteristic peaks of gypsum at 3580 cm^{-1}, 3430 cm^{-1}, and 1108 cm^{-1} were not detected. Instead, the spectra resembled those of the humic acid- and alginate-conditioned membranes before gypsum scaling (Fig. S5B) by exhibiting the characteristic peaks of humic acid (1635 cm^{-1} and 1419 cm^{-1}) and alginate (1600-1500 cm^{-1} and 1400 cm^{-1}). These results indicate that gypsum formation was largely hindered on the foulant layer consisting of humic acid or alginate. Further, the spectra of BSA-conditioned membrane

showed the dampened peaks corresponding to gypsum in addition to those from BSA (N–C═O, 1700-1600 cm^{-1}) and the TFC-PA membrane (Fig. S6, Supplementary Materials), while only gypsum-related peaks were observed for the lysozyme-conditioned membrane. This further supports that BSA conditioning inhibited gypsum scale formation while lysozyme conditioning posed no effect.

The crystalline structures of the scales formed on the conditioned membranes were analyzed by XRD (Fig. 5H). The XRD peaks associated with the (020), (021), (040), and (041) facets of gypsum crystal were dramatically reduced for the humic acid-, alginate-, and BSA-conditioned membranes, consistent with the inhibiting effect of these foulant layers on gypsum formation as revealed by FTIR (Fig. 5G). Although the peak intensities were low due to the limited number of gypsum crystals on top of the surface, we were still able to calculate the peak intensity ratio of (020) to (021) facets. As listed in Table S1, the value of peak ratio changed from 0.7 (control) to 1.2, 1.0, 0.3, and 3.6 for humic acid-, alginate-, lysozyme-, and BSA-conditioned membranes, respectively, consistent with the observation in combined organic fouling and gypsum scaling (Method 1). This consistency provides the evidence that the gypsum crystal formation during combined fouling and scaling experiment was dominated by surface nucleation (more evidence will be provided on this statement in the following sections). We noticed that lysozyme induced different extents of peak ratio reduction between Method 1 and Method 2 (transitioning from a peak ratio of 0.7 for the control to 0.6 and 0.3 for Method 1 and Method 2, respectively). This variation in the degree of crystal distortion was likely because more lysozyme was deposited during lysozyme conditioning than Method 1. Furthermore, the peak ratio was decreased by lysozyme but increased by the other foulants (Table S1). Such a difference might be due to the distinct adsorption preference of the foulants onto various gypsum crystal facets [41], thereby exhibiting different impacts of crystal distortion.

We also performed XPS analysis on the conditioned membranes after gypsum scaling to investigate the chemical environment of calcium element. As displayed in Fig. 5I, the characteristic peaks of Ca $2p_{3/2}$ and Ca $2p_{1/2}$ for foulant-conditioned membranes were shifted towards lower binding energies compared with the control. As mentioned earlier in Section 3.1, the shifts to lower binding energies were likely ascribed to $Ca–COO^-$ bindings resulting from the organic foulants. In the case of lysozyme conditioning, specifically, the peak positions were moderately shifted from 349.5 eV to 353.1 eV–349.0 eV and 352.6 eV for Ca $2p_{3/2}$ and Ca $2p_{1/2}$, respectively (Table S2). Moreover, the foulant-conditioned surfaces showing foulant layers (i.e., humic acid, alginate, and BSA) with little to no formation of gypsum scales exhibited significant shifts of peak positions to around 347.5 eV and 351.2 eV, respectively.

Furthermore, the decompositions of the Ca $2p_{3/2}$ peaks into subpeaks of different calcium bindings are shown in Fig. 6. According to the spectra for humic acid- and alginate-conditioned membranes after gypsum scaling (Fig. 6B and C), only $Ca–COO^-$ binding was observed while both $Ca–SO_4$ and $Ca–COO^-$ bindings were present for the pristine (Fig. 6A) membrane as well as lysozyme- and BSA-conditioned membranes (Fig. 6D and E). Considering the depth of XPS analysis (only 5–10 nm) [28,34], it is not surprising that $Ca–SO_4$ binding was not observed even though gypsum was present underneath the foulant layers of humic acid and alginate, as detected by the other characterization techniques such as SEM, ATR-FTIR, and XRD (Fig. 5G-I). Additionally, a small peak for $Ca–SO_4$ binding appeared for the BSA-conditioned membrane, which was in accordance with the small amount of gypsum scale observed on the BSA conditioned surface. The contributions of these two types of Ca bindings were further examined by the relative abundance of each binding (Fig. 6F). The relative abundance of $Ca–SO_4$ binding (resulting from gypsum formation) was in the order of pristine membrane $\geq$ lysozyme-conditioned membrane $>$ BSA-conditioned membrane $>$ humic acid-conditioned membrane $=$ alginate-conditioned membrane. These XPS results, along with the FTIR and XRD results, suggest unequivocally that a thick foulant layer of humic acid or alginate hinders gypsum formation on the membrane surface significantly. However, gypsum scales were found on the surface after combined humic acid/alginate fouling and gypsum scaling (i.e.,

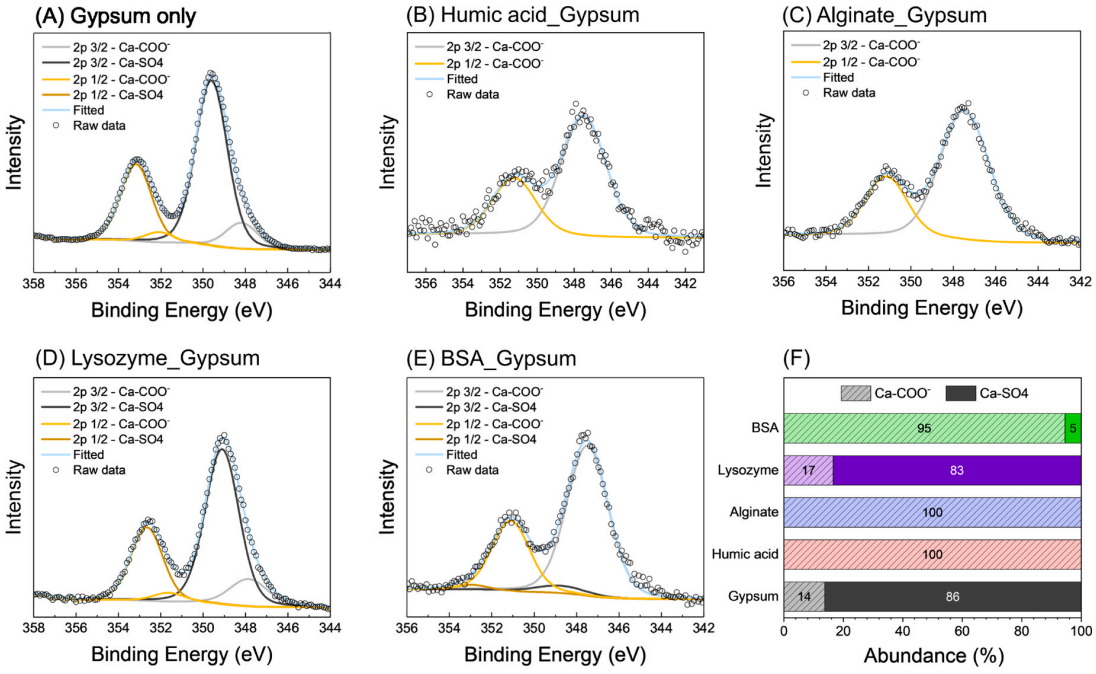

Fig. 6. High-resolution XPS spectral decompositions of Ca 2p to subpeaks of $Ca–SO_4$ and $Ca–COO^-$ bindings. Membrane surfaces after gypsum scaling on (A) pristine membrane, (B) humic acid-conditioned membrane, (C) alginate-conditioned membrane, (D) lysozyme-conditioned membrane, and (E) BSA-conditioned membrane. (F) Relative abundance of $Ca–COO^-$ and $Ca–SO_4$ bindings by calculating the peak areas. The sum of the two binding types is designated as 100 %.

Method 1, Fig. 2), inferring that organic foulants present in the bulk solution led to different gypsum scaling behaviors from the scenarios where a thick foulant layer was already formed on the membrane surface (i.e., Method 2). To expound, at the early stage during combined fouling and scaling experiments (Method 1), foulants in the bulk solution formed a foulant layer on the membrane surface and this layer was able to facilitate gypsum formation by the cake enhanced concentration polarization similar to what was observed in Method 2. However, at the later stage, as the foulant layer was not as thick as Method 2, the gypsum crystals were able to grow over the foulant layer. Consequently, both the gypsum scales and the foulant layer were found on the surface after combined fouling and scaling as depicted by Fig. 2.

3.3. The effects of organic foulants on gypsum formation in the bulk solutions

In addition to dynamic RO experiments, static experiments were carried out to investigate the behaviors of gypsum formation in the bulk solutions in the presence of organic foulants. By doing so, we were able to decouple the effects of organic foulants on bulk nucleation from those on surface nucleation of gypsum. As shown in Fig. 7, when the static experiment was performed without any foulant, the solution conductivity started to decrease at ~100 min when the formation of gypsum scale (which consumed precursor ions) occurred. However, the induction time of gypsum formation was postponed in the presence of organic foulants. Specifically, humic acid, BSA, alginate, and lysozyme extended the induction of gypsum formation to 3,000, 800, 500 and 120 min, respectively. Several studies [18,19] have shown that organic molecules with carboxyl groups were able to inhibit gypsum formation in the bulk solution. The carboxylic acidities of alginate, humic acid and BSA, which represent the density of carboxylic acid groups, have been reported as 3.5, 3.4, and 1 mequiv g^{-1}, respectively [42], and lysozyme is known to have a smaller number of carboxyl groups than BSA [43,44]. Therefore, the order of carboxyl group acidity does not match that of induction time of gypsum formation, and there must be other factors affecting bulk nucleation of gypsum (such as molecular size and structure). Further, we noticed that the extension of induction time does not accord with the results of dynamic RO experiment, providing additional evidence that bulk nucleation is not the dominating mechanism that governs water flux decline during combined organic fouling and gypsum scaling.

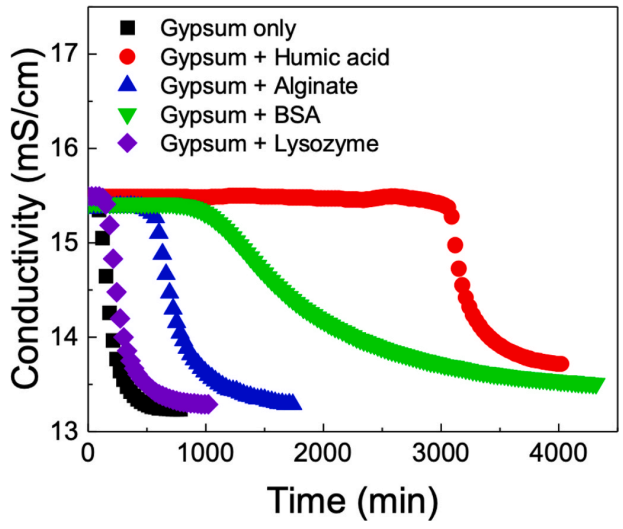

Fig. 7. Solution conductivity as a function of time during static experiments of gypsum formation. The solutions contained 42 mM $CaCl_2{\cdot}2H_2O$ and 42 mM Na_2SO_4 as gypsum precursors, as well as 20 mg L^{-1} foulants (if added). The tests were carried out under room temperature until the stable conductivity was reached.

We notice that different proteins (i.e., BSA and lysozyme) posed varied effects on gypsum scaling in all three sets of experiments in our study, which indicates that molecular properties of protein are likely to regulate the impact of protein on the scaling behavior. To further explore this phenomenon, we probed the effects of several amino acids on gypsum scaling because (1) proteins are composed of amino acid as building blocks, and (2) the properties of amino acids are simpler and more controlled than proteins. Specifically, we selected two negatively charged amino acids (aspartic acid and glutamic acid) and one positively charged amino acid (arginine). Aspartic acid is known to be present in both proteins, while glutamic acid and arginine are the major constituents of BSA and lysozyme, respectively [45,46]. As shown in Fig. S7 (Supplementary Materials), the presence of these three amino acids did not significantly affect the gypsum scaling behaviors during both dynamic and static experiments. Therefore, despite the fact that BSA and lysozyme are well known to carry different surface charges (negatively charge for BSA vs. positive charge for lysozyme at near neutral pH) [47,48], surface charge alone could not be the primary driving factor for the observed differences in the behaviors of combined protein fouling and gypsum scaling. Rather, other properties of the proteins (e.g., the molecular conformation and the molecular size) might play an important role in regulating protein-gypsum interactions, warranting future research to further unravel the underlying mechanism. Such a hypothesis is analogous to findings in the field of biomolecules, where different anti-freeze proteins, which allow cells to survive in sub-zero conditions by altering ice crystal growth behaviors, showed varied bindings to different ice crystal planes, resulting in different growth rate of ice crystals depending on the structure of the proteins [49–51].

The gypsum crystals collected from the static experiments were characterized by SEM and XRD (Fig. 8). The gypsum crystals formed in the absence of organic foulants exhibited needle-like morphologies with high aspect ratios (Fig. 8A), with alginate and lysozyme not causing significant morphological alteration (Fig. 8C and E). However, in the presence of humic acid and BSA, polygon-like gypsum crystals were observed (Fig. 8B and D with inset images). This morphological change might be attributed to the greater extent of adsorption of humic acid and BSA to gypsum surface than that of alginate (as evidenced by Figs. 7 and 8F) as the adsorbed molecules could disrupt crystal formation by restraining growth along the orientations of the reactive facets [18,41]. Furthermore, it is reported that humic acid and BSA possess a globular structure [52,53] while alginate has a linear structure [54]. The scale inhibitor with a three-dimensional structure altered morphology of scales and exhibited better efficiency in scaling inhibition than that with a linear structure [55]. Thus, such crystal distortion posed by humic acid and BSA was consistent with the most significant effect of these two organic foulants on the induction time of gypsum formation. Furthermore, we observed significant morphological changes in gypsum crystals with alginate in the dynamic experiments using Method 1 (Fig. 2C), in contrast to the static experiments where such changes were absent (Fig. 8C). This discrepancy suggests that gypsum crystal growth was not primarily influenced by the foulants in the bulk solution. Instead, our observations support the notion that the foulant layer on the membrane surface had a greater influence on gypsum scaling than the foulants in the bulk solution during combined alginate fouling and gypsum scaling.

Further, the XRD results (Fig. 8F) showed that the gypsum scales formed in the bulk solution without organic foulants exhibited characteristic peaks of gypsum with a high intensity for the (020) facet and a low intensity for the (021) facet. However, the peak intensity for the (020) facet was reduced dramatically in the presence of humic acid and BSA, indicating gypsum growth along the orientation of (020) facet was greatly inhibited by the foulants. Such changes in peak intensity were distinguished from those observed in dynamic RO experiments (Figs. 2H and 5H). As shown in Table S1, the peak intensity ratio of (020)/(021) facets for gypsum crystals formed in the presence of foulants were greatly reduced compared to the control during static experiment, in

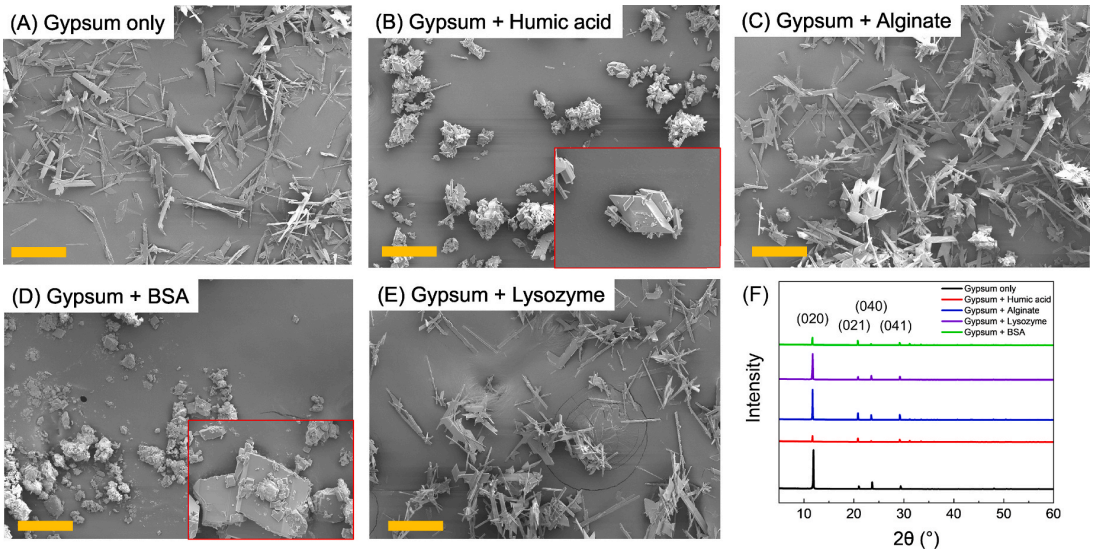

Fig. 8. SEM images (obtained at the magnification of × 200) of the gypsum crystals during static experiments (A) without organic foulant, with (B) humic acid, (C) alginate, (D) BSA, and (E) lysozyme. The scale bar represents 100 μm and the inserted images in (B and D) were taken at a higher magnification (× 2000). (F) XRD spectra of the gypsum crystals.

contrast to the generally increased ratios observed in dynamic combined fouling and scaling (i.e., Method 1, except for gypsum with lysozyme). It is worth mentioning that the results from Method 1 of dynamic experiments were consistent with those of Method 2 (i.e., conditioned membranes in dynamic scaling experiments) that represents surface phenomenon, as explained in Section 3.2. Therefore, this result suggests again that the gypsum crystal growth during combined organic fouling and gypsum scaling was influenced more by the foulant layer formed on the membrane surface (i.e., surface-induced nucleation) than by the foulants that were present in the bulk solution.

To assess the changes in chemical properties of the gypsum crystals formed in the presence of organic foulants, XPS and ATR-FITR techniques were employed on the precipitates collected from static experiment (Fig. S8, Supplementary Materials). The XPS results (Fig. S8A and Table S2) showed that the gypsum crystals formed with organic foulants did not exhibit noticeable shifts in the binding energies of Ca $2p_{3/2}$ and Ca $2p_{1/2}$ when compared to gypsum crystals formed without foulants. This result implies that chemical bindings between calcium and foulant did not take place, consistent with what was observed by Cao et al. [18] Such a conclusion is also supported by the FTIR spectra of all the samples, which only exhibited the presence of gypsum characteristic peaks (Fig. S8B). These results of FTIR and XPS analyses demonstrate that foulants likely affected gypsum formation in the bulk solution by physically adsorbing onto the surface of the gypsum crystals, rather than forming strong chemical bonds. In addition, the difference in the ATR-FTIR and XPS results between dynamic and static experiments further supports the notion that bulk nucleation is not the major governing mechanism of combined fouling and scaling.

4. Conclusions

In this study, we have performed a comprehensive investigation to decouple the surface and bulk phenomena of combined organic fouling and gypsum scaling in the RO process. Dynamic RO experiments were conducted using two methods (e.g., Method 1 - combined fouling and scaling, Method 2 - gypsum scaling on organic-conditioned membranes) in a crossflow RO system, while static experiments were performed without a membrane. The behaviors of combined fouling and scaling aligned more with Method 2 of the dynamic experiment, which reveals the effect of foulant layer on surface-induced gypsum nucleation, but contrasted with the results from static experiment that represents bulk nucleation. These findings, along with detailed gypsum characterizations, provide compelling evidence that supports the prominence of surface nucleation as the dominant mechanism governing the complex phenomena of combined organic fouling and gypsum scaling. Recognizing surface nucleation as the prevailing mechanism has the potential to guide the development of effective strategies for fouling and scaling control in RO process, such as surface modifications for fouling-resistant membranes that are able to hinder foulant attachment and to deter surface nucleation of gypsum. In addition, we are aware of existing publications where the effects of multivalent ions (especially Ca^{2+}) on organic fouling were investigated [7,11,56]. Thus, it is worth mentioning that the findings of this work are fundamentally distinct from the results of these studies, because we are exploring the effects of organic foulants on nucleation and crystal growth of gypsum.

Furthermore, BSA exhibited remarkable effectiveness in hindering gypsum scaling during combined fouling and scaling. This result explains the lack of gypsum scales on fouled membranes after real RO treatment of secondary municipal wastewater effluent where proteins commonly exist [56,57], as shown by several recent publications [58,59]. Our results also suggest the potential of harnessing BSA or organic compounds with similar structural features as additives to feedwater, offering an environmentally friendly approach to address the issue of mineral scaling. Alternatively, the removal of BSA-like proteins in pretreatment might pose a facilitating (rather than mitigating) effect on gypsum scaling in RO desalination. Retaining these proteins in the feedwater after pretreatment could serve as a strategy of mitigating scaling. Interestingly, no observable mitigating effect was seen for lysozyme, another protein possessing different structural features from BSA. This result implies that structural features are likely to play a significant role in influencing the effects of organic macromolecules on mineral scaling. Future studies should aim to further explore this aspect by leveraging advanced techniques such as molecular simulations and synthetic biology to further unravel the intricate interplay between foulant characteristics and scaling behaviors. In addition, it is worthy to assess the effect of organic foulants on mineral scaling in the presence of multiple organic foulants. Such assessment will involve dedicated research delving into the complex foulant-scalant and foulant-foulant interplays, which are valuable to expand the findings of the current study. Such explorations would offer the potential to unlock innovative

strategies for fouling and scaling control to improve the efficiency and viability of RO desalination.

CRediT authorship contribution statement

Shinyun Park: Writing – review & editing, Writing – original draft, Validation, Methodology, Investigation, Formal analysis, Data curation, Conceptualization. **Mayca Saavedra:** Data curation. **Xitong Liu:** Writing – review & editing, Methodology. **Tianshu Li:** Writing – review & editing, Methodology. **Bridget Anger:** Writing – review & editing. **Tiezheng Tong:** Writing – review & editing, Validation, Supervision, Resources, Project administration, Funding acquisition, Conceptualization.

Declaration of competing interest

The authors declare that they have no known competing financial interests or personal relationships that could have appeared to influence the work reported in this paper.

Data availability

Data will be made available on request.

Acknowledgement

This material is based upon work supported by the National Science Foundation under Grant No. 2143508 and 2143970.

Appendix A. Supplementary data

Supplementary data to this article can be found online at https://doi.org/10.1016/j.memsci.2023.122399.

References

[1] The United Nations World Water Development Report 2023: Partnerships and Cooperation for Water, UNESCO World Water Assessment, 2023.
[2] S.N. Haq, Global Water Crisis Could 'spiral Out of Control' Due to Overconsumption and Climate Change, UN Report Warns, 2023. https://www.cnn.com/2023/03/22/world/global-water-crisis-un-report-climate-intl/index.html. (Accessed 2 October 2023).
[3] M. Elimelech, W.A. Phillip, The future of seawater desalination: energy, technology, and the environment, Science 333 (6043) (2011) 712–717, https://doi.org/10.1126/science.1200488.
[4] L.F. Greenlee, D.F. Lawler, B.D. Freeman, B. Marrot, P. Moulin, Reverse osmosis desalination: water sources, technology, and today's challenges, Water Res. 43 (9) (2009) 2317–2348, https://doi.org/10.1016/j.watres.2009.03.010.
[5] S.S. Shenvi, A.M. Isloor, A. Ismail, A review on RO membrane technology: Developments and challenges, Desalination 368 (2015) 10–26, https://doi.org/10.1016/j.desal.2014.12.042.
[6] G. Amy, Fundamental understanding of organic matter fouling of membranes, Desalination 231 (1–3) (2008) 44–51, https://doi.org/10.1140/epjp/i2017-11531-8.
[7] Q.L. Li, M. Elimelech, Organic fouling and chemical cleaning of nanofiltration membranes: measurements and mechanisms, Environ. Sci. Technol. 38 (17) (2004) 4683–4693, https://doi.org/10.1021/es0354162.
[8] S. Shirazi, C.-J. Lin, D. Chen, Inorganic fouling of pressure-driven membrane processes—a critical review, Desalination 250 (1) (2010) 236–248, https://doi.org/10.1016/j.desal.2009.02.056.
[9] T.Z. Tong, A.F. Wallace, S. Zhao, Z. Wang, Mineral scaling in membrane desalination: mechanisms, mitigation strategies, and feasibility of scaling-resistant membranes, J. Membr. Sci. 579 (2019) 52–69, https://doi.org/10.1016/j.memsci.2019.02.049.
[10] D. Sioutopoulos, A. Karabelas, S. Yiantsios, Organic fouling of RO membranes: investigating the correlation of RO and UF fouling resistances for predictive purposes, Desalination 261 (3) (2010) 272–283, https://doi.org/10.1016/j.desal.2010.06.071.
[11] S. Lee, M. Elimelech, Relating organic fouling of reverse osmosis membranes to intermolecular adhesion forces, Environ. Sci. Technol. 40 (3) (2006) 980–987, https://doi.org/10.1021/es051825h.
[12] B. Mi, M. Elimelech, Silica scaling and scaling reversibility in forward osmosis, Desalination 312 (2013) 75–81, https://doi.org/10.1016/j.desal.2012.08.034.
[13] B.X. Mi, M. Elimelech, Gypsum scaling and cleaning in forward osmosis: measurements and mechanisms, Environ. Sci. Technol. 44 (6) (2010) 2022–2028, https://doi.org/10.1021/es903623r.
[14] T. Tran, B. Bolto, S. Gray, M. Hoang, E. Ostarcevic, An autopsy study of a fouled reverse osmosis membrane element used in a brackish water treatment plant, Water Res. 41 (17) (2007) 3915–3923, https://doi.org/10.1016/j.watres.2007.06.008.
[15] H.L. Yang, C. Huang, J.R. Pan, Characteristics of RO foulants in a brackish water desalination plant, Desalination 220 (1–3) (2008) 353–358, https://doi.org/10.1016/j.desal.2007.01.040.
[16] J. Wang, L. Wang, R. Miao, Y. Lv, X. Wang, X. Meng, R. Yang, X. Zhang, Enhanced gypsum scaling by organic fouling layer on nanofiltration membrane: characteristics and mechanisms, Water Res. 91 (2016) 203–213, https://doi.org/10.1016/j.watres.2016.01.019.
[17] M. Wang, B. Cao, Y.D. Hu, D.F. Rodrigues, Mineral scaling on reverse ssmosis membranes: role of mass, orientation, and crystallinity on permeability, Environ. Sci. Technol. 55 (23) (2021) 16110–16119, https://doi.org/10.1021/acs.est.1c04143.
[18] T.C. Cao, J. Rolf, Z.X. Wang, C. Violet, M. Elimelech, Distinct impacts of natural organic matter and colloidal particles on gypsum crystallization, Water Res. 218 (2022) 9, https://doi.org/10.1016/j.watres.2022.118500.
[19] J. Benecke, J. Rozova, M. Ernst, Anti-scale effects of select organic macromolecules on gypsum bulk and surface crystallization during reverse osmosis desalination, Sep. Purif. Technol. 198 (2018) 68–78, https://doi.org/10.1016/j.seppur.2016.11.068.
[20] J. Rolf, T. Cao, X. Huang, C. Boo, Q. Li, M. Elimelech, Inorganic scaling in membrane desalination: models, mechanisms, and characterization methods, Environ. Sci. Technol. 56 (12) (2022) 7484–7511, https://doi.org/10.1021/acs.est.2c01858.
[21] Y.L. Liu, B.X. Mi, Effects of organic macromolecular conditioning on gypsum scaling of forward osmosis membranes, J. Membr. Sci. 450 (2014) 153–161, https://doi.org/10.1016/j.memsci.2013.09.001.
[22] Y. Yin, S. Kalam, J.L. Livingston, R. Minjarez, J. Lee, S. Lin, T. Tong, The use of anti-scalants in gypsum scaling mitigation: comparison with membrane surface modification and efficiency in combined reverse osmosis and membrane distillation, J. Membr. Sci. 643 (2022) 120077, https://doi.org/10.1016/j.memsci.2021.120077.
[23] S.-H. Yoon, C.-H. Lee, K.-J. Kim, A.G. Fane, Effect of calcium ion on the fouling of nanofilter by humic acid in drinking water production, Water Res. 32 (7) (1998) 2180–2186, https://doi.org/10.1016/S0043-1354(97)00416-8.
[24] M. Uchymiak, E. Lyster, J. Glater, Y. Cohen, Kinetics of gypsum crystal growth on a reverse osmosis membrane, J. Membr. Sci. 314 (1–2) (2008) 163–172, https://doi.org/10.1016/j.memsci.2008.01.041.
[25] M.Y. Ashfaq, M.A. Al-Ghouti, D.A. Da'na, H. Qiblawey, N. Zouari, Effect of concentration of calcium and sulfate ions on gypsum scaling of reverse osmosis membrane, mechanistic study, J. Mater. Res. Technol. 9 (6) (2020) 13459–13473, https://doi.org/10.1016/j.jmrt.2020.09.117.
[26] S.J. McClellan, E.I. Franses, Adsorption of bovine serum albumin at solid/aqueous interfaces, Colloids Surf. A Physicochem. Eng. Asp. 260 (1–3) (2005) 265–275, https://doi.org/10.1016/j.colsurfa.2005.03.017.
[27] M. Inoue, I. Hirasawa, The relationship between crystal morphology and XRD peak intensity on CaSO4· 2H2O, J. Cryst. Growth 380 (2013) 169–175, https://doi.org/10.1016/j.jcrysgro.2013.06.017.
[28] F.A. Stevie, C.L. Donley, Introduction to x-ray photoelectron spectroscopy, J. Vac. Sci. Technol. A 38 (6) (2020) 063204, https://doi.org/10.1116/6.0000412.
[29] A.E. Contreras, Z. Steiner, J. Miao, R. Kasher, Q. Li, Studying the role of common membrane surface functionalities on adsorption and cleaning of organic foulants using QCM-D, Environ. Sci. Technol. 45 (15) (2011) 6309–6315, https://doi.org/10.1021/es200570t.
[30] X. Jin, X. Huang, E.M. Hoek, Role of specific ion interactions in seawater RO membrane fouling by alginic acid, Environ. Sci. Technol. 43 (10) (2009) 3580–3587, https://doi.org/10.1021/es8036498.
[31] A. Christie, J. Lee, I. Sutherland, J. Walls, An XPS study of ion-induced compositional changes with group II and group IV compounds, Appl. Surf. Sci. 15 (1–4) (1983) 224–237, https://doi.org/10.1016/0378-5963(83)90018-1.
[32] B. Demri, D. Muster, XPS study of some calcium compounds, J. Mater. Process. Technol. 55 (3–4) (1995) 311–314, https://doi.org/10.1016/0924-0136(95)02023-3.
[33] A. Achour, A. Arman, M. Islam, A. Zavarian, A. Basim Al-Zubaidi, J. Szade, Synthesis and characterization of porous CaCO3 micro/nano-particles, Eur. Phys. J. Plus 132 (6) (2017) 267, https://doi.org/10.1140/epjp/i2017-11531-8.
[34] S. Kerber, T. Barr, G. Mann, W. Brantley, E. Papazoglou, J. Mitchell, The complementary nature of X-ray photoelectron spectroscopy and angle-resolved X-ray diffraction part I: background and theory, J. Mater. Eng. Perform. 7 (1998) 329–333, https://doi.org/10.1361/105994998770347765.
[35] S.G. Kazarian, K.A. Chan, ATR-FTIR spectroscopic imaging: recent advances and applications to biological systems, Analyst 138 (7) (2013) 1940–1951, https://doi.org/10.1039/c3an36865c.
[36] X. Tong, Y.-H. Wu, Y.-H. Wang, Y. Bai, X.-H. Zhao, L.-W. Luo, Y. Mao, N. Ikuno, H.-Y. Hu, Simulating and predicting the flux change of reverse osmosis membranes over time during wastewater reclamation caused by organic fouling, Environ. Int. 140 (2020) 105744, https://doi.org/10.1016/j.envint.2020.105744.
[37] R. Shang, H.p. Deng, J.y. Hu, Removal of humic acid by a new type of electrical hollow-fiber microfiltration (E-HFMF), AIP Conf. Proc. 1251 (1) (2010) 97–100, https://doi.org/10.1063/1.3529353.

[38] R. Pereira, A. Tojeira, D.C. Vaz, A. Mendes, P. Bártolo, Preparation and characterization of films based on alginate and aloe vera, Int. J. Polym. Anal. Char. 16 (7) (2011) 449–464, https://doi.org/10.1080/1023666X.2011.599923.
[39] E.M.V. Hoek, M. Elimelech, Cake-enhanced concentration polarization: a new fouling mechanism for salt-rejecting membranes, Environ. Sci. Technol. 37 (24) (2003) 5581–5588, https://doi.org/10.1021/es0262636.
[40] Z.S. Yan, F.S. Qu, H. Liang, H.R. Yu, H.L. Pang, H.W. Rong, G.D. Fan, B. Van der Bruggen, Effect of biopolymers and humic substances on gypsum scaling and membrane wetting during membrane distillation, J. Membr. Sci. 617 (2021) 118638, https://doi.org/10.1016/j.memsci.2020.118638.
[41] Y.M. Yin, N. Jeong, R. Minjarez, C.A. Robbins, K.H. Carlson, T.Z. Tong, Contrasting behaviors between gypsum and silica Scaling in the presence of antiscalants during membrane distillation, Environ. Sci. Technol. 55 (8) (2021) 5335–5346, https://doi.org/10.1021/acs.est.0c07190.
[42] B. Mi, M. Elimelech, Chemical and physical aspects of organic fouling of forward osmosis membranes, J. Membr. Sci. 320 (1–2) (2008) 292–302, https://doi.org/10.1016/j.memsci.2008.04.036.
[43] T.-Y. Lin, D. Koshland Jr., Carboxyl group modification and the activity of lysozyme, J. Biol. Chem. 244 (2) (1969) 505–508, https://doi.org/10.1016/s0021-9258(18)94459-5.
[44] G.T. Hermanson, Bioconjugate Techniques, Academic press, 2013, https://doi.org/10.1016/c2009-0-64240-9.
[45] S. Pacheco, J. Oiano-Neto, R.L.D.O. Godoy, J.S.D. Rosa, R. De Souza, Amino acids analysis by RP-HPLC and derivatization with 6-aminoquinolyl-N-hydroxysuccnimidyl carbamate (AQC) using bovine serum albumin (BSA) for method standardization, CIGR - International Conference of Agricultural Engineering, Brazil, August 31 to September 4 (2008).
[46] G. Yan, G. Nyquist, K.D. Caldwell, R. Payor, E. McCraw, Quantitation of total protein deposits on contact lenses by means of amino acid analysis, Investig. Ophthalmol. Vis. Sci. 34 (5) (1993) 1804–1813.
[47] A.N. Quay, T.Z. Tong, S.M. Hashmi, Y. Zhou, S. Zhao, M. Elimelech, Combined organic fouling and inorganic scaling in reverse osmosis: role of protein-silica interactions, Environ. Sci. Technol. 52 (16) (2018) 9145–9153, https://doi.org/10.1021/acs.est.8b02194.
[48] Y.-N. Wang, C.Y. Tang, Fouling of nanofiltration, reverse osmosis, and ultrafiltration membranes by protein mixtures: the role of inter-foulant-species interaction, Environ. Sci. Technol. 45 (15) (2011) 6373–6379, https://doi.org/10.1021/es2013177.
[49] A. Eskandari, T.C. Leow, M.B.A. Rahman, S.N. Oslan, Antifreeze proteins and their practical utilization in industry, medicine, and agriculture, Biomolecules 10 (12) (2020) 1649, https://doi.org/10.3390/biom10121649.
[50] Z. Jia, C.I. DeLuca, H. Chao, P.L. Davies, Structural basis for the binding of a globular antifreeze protein to ice, Nature 384 (6606) (1996) 285–288, https://doi.org/10.1038/384285a0.
[51] G. Gharib, S. Saeidiharzand, A.K. Sadaghiani, A. Koşar, Antifreeze proteins: a tale of evolution from origin to energy applications, Front. Bioeng. Biotechnol. 9 (2022) 770588, https://doi.org/10.3389/fbioe.2021.770588.
[52] S.C.B. Myneni, J. Brown, G. Martinez, W. Meyer-Ilse, Imaging of humic substance macromolecular structures in water and soils, Science 286 (5443) (1999) 1335–1337, https://doi.org/10.1126/science.286.5443.1335.
[53] C.Y. Tang, T. Chong, A.G. Fane, Colloidal interactions and fouling of NF and RO membranes: a review, Adv. Colloid Interface Sci. 164 (1–2) (2011) 126–143, https://doi.org/10.1016/j.cis.2010.10.007.
[54] H.S. Kim, C.-G. Lee, E.Y. Lee, Alginate lyase: structure, property, and application, Biotechnol. Bioproc. Eng. 16 (2011) 843–851, https://doi.org/10.1007/s12257-011-0352-8.
[55] H. Huang, Q. Yao, Q. Jiao, B. Liu, H. Chen, Polyepoxysuccinic acid with hyperbranched structure as an environmentally friendly scale inhibitor and its scale inhibition mechanism, J. Saudi Chem. Soc. 23 (1) (2019) 61–74, https://doi.org/10.1016/j.jscs.2018.04.003.
[56] P.J. Westgate, C. Park, Evaluation of proteins and organic nitrogen in wastewater treatment effluents, Environ. Sci. Technol. 44 (14) (2010) 5352–5357, https://doi.org/10.1021/es100244s.
[57] R.D. Holbrook, J. Breidenich, P.C. DeRose, Impact of reclaimed water on select organic matter properties of a receiving stream fluorescence and perylene sorption behavior, Environ. Sci. Technol. 39 (17) (2005) 6453–6460, https://doi.org/10.1021/es047971p.
[58] B. Abada, S. Joag, B. Alspach, A. Bustamante, S. Chellam, Inorganic and organic silicon fouling of nanofiltration membranes during pilot-scale direct potable reuse, ACS ES&T Eng. 3 (9) (2023) 1413–1423, https://doi.org/10.1021/acsestengg.3c00172.
[59] V.A. Niemann, M. Huck, H.-G. Steinrück, M.F. Toney, W.A. Tarpeh, S.E. Bone, X-ray absorption spectroscopy reveals mechanisms of calcium and silicon fouling on reverse osmosis membranes used in wastewater reclamation, ACS ES&T Water 3 (8) (2023) 2627–2637, https://doi.org/10.1021/acsestwater.3c00144.